4354 J. Med. Chem. 2010, 53, 4354–4366
DOI: 10.1021/jm9013899

Journal of Medicinal Chemistry Article

Structural Insight into Peroxisome Proliferator-Activated Receptor γ Binding of Two Ureidofibrate-Like Enantiomers by Molecular Dynamics, Cofactor Interaction Analysis, and Site-Directed Mutagenesis

Giorgio Pochetti,[†,◆] Nico Mitro,[‡,§,◆] Antonio Lavecchia,[∥,◆] Federica Gilardi,[‡,¶] Neva Besker,[⊥] Elena Scotti,[‡,+] Massimiliano Aschi,[#] Nazzareno Re,[⊥] Giuseppe Fracchiolla,[▽] Antonio Laghezza,[▽] Paolo Tortorella,[▽] Roberta Montanari,[†] Ettore Novellino,[∥] Fernando Mazza,[†,○] Maurizio Crestani,[*,‡,◆] and Fulvio Loiodice[*,▽,◆]

[†]*Istituto di Cristallografia, Consiglio Nazionale delle Ricerche, Montelibretti, 00015 Monterotondo Stazione, Roma, Italia,* [‡]*Laboratorio "Giovanni Galli" di Biochimica e Biologia Molecolare dei Lipidi e Spettrometria di Massa, and* [§]*Laboratorio "Giovanni Armenise-Harvard Foundation", Dipartimento di Scienze Farmacologiche, Università degli Studi di Milano, 20133 Milano, Italia,* [∥]*Dipartimento di Chimica Farmaceutica e Tossicologica, Università degli Studi di Napoli "Federico II", 80131 Napoli, Italia,* [⊥]*Dipartimento di Scienze del Farmaco, Università "G. D'Annunzio", 06100 Chieti, Italia,* [#]*Dipartimento di Chimica, Ingegneria Chimica e Materiali, Università di L'Aquila, 67010 L'Aquila, Italia,* [▽]*Dipartimento Farmaco-Chimico, Università degli Studi di Bari "Aldo Moro", 70126 Bari, Italia, and* [○]*Dipartimento di Scienze della Salute, Università di L'Aquila, 67010 L'Aquila, Italia.* [◆] *These authors contributed equally to this work.* [¶] *Current address: University of Lausanne, Center for Integrative Genomics, Genopode Building, Room 5010, 1015 Lausanne, Switzerland.* [+] *Current address: Department of Pathology and Laboratory Medicine/Howard Hughes Medical Institutes, University of California at Los Angeles, Los Angeles, California.*

Received September 18, 2009

Molecular dynamics simulations were performed on two ureidofibrate-like enantiomers to gain insight into their different potency and efficacy against PPARγ. The partial agonism of the *S* enantiomer seems to be due to its capability to stabilize different regions of the receptor allowing the interaction with both coactivators and corepressors as shown by fluorescence resonance energy transfer (FRET) assays. The recruitment of the corepressor N-CoR1 by the *S* enantiomer on two different responsive elements of PPARγ regulated promoters was confirmed by chromatin immunoprecipitation assays. Cell-based transcription assays show that PPARγ coactivator 1α (PGC-1α) and cAMP response element binding protein-binding protein (CBP) enhance the basal and ligand-stimulated receptor activity acting as coactivators of PPARγ, whereas the receptor interacting protein 140 (RIP140) and the nuclear corepressor 1 (N-CoR1) repress the transcriptional activity of PPARγ. We also tested the importance of the residue Q286 on the transcriptional activity of the receptor by site-directed mutagenesis and confirmed its key role in the stabilization of helix 12. Molecular modeling studies were performed to provide a molecular explanation for the different behavior of the mutants.

Introduction

Peroxisome proliferator-activated receptor γ (PPARγ)[a] belongs to the nuclear receptor (NR) superfamily of ligand-activated transcription factors. PPARγ is a member of the NR1C subgroup that includes PPARα and PPARβ/δ forming a subfamily of "lipid sensing" receptors that regulate important aspects of lipid and glucose homeostasis.[1,2] PPARγ is the most extensively studied among the PPAR subtypes and plays important roles in the functions of adipocytes, muscles, and macrophages with a direct impact on type 2 diabetes, dyslipidemia, atherosclerosis, and cardiovascular diseases.[3,4]

The first insight into the link between PPARγ and diabetes came from the discovery of PPARγ as the biologic target for the thiazolidinedione class of antidiabetic drugs (TZDs).[5,6] TZDs are effective insulin sensitizers and have been shown to improve glucose uptake and lower hyperglycaemia and hyperinsulinaemia.[6−9] However, as full agonists they also stimulate adipocyte differentiation in vitro and weight gain in vivo, which normally aggravates the diabetic state. Additional undesirable side effects associated with TZD treatment include edema/hemodilution, cardiomegaly, anemia, and increased incidence of bone fractures.[10,11]

As a result of the clinical observations mentioned above, emphasis has shifted to the development of partial agonists or selective PPARγ modulators (SPPARγMs). These new ligands, although displaying reduced transcriptional activity in reporter assays, exhibit robust antidiabetic efficacy with improved tolerability.[12−15]

Previously published data seem to indicate that the unique properties of partial agonists may be due to their distinct physical interaction with the receptor. Indeed, X-ray cocrystallographic studies of the PPARγ ligand binding domain (LBD) complexed with full agonists indicate the critical role of

*To whom correspondence should be addressed. Phone: +39 080-5442798, Fax: +39 080-5442231, Email: floiodice@farmchim.uniba.it; Phone: +39 02-50318393, Fax: +39 02-50318391, Email: maurizio.crestani@unimi.it.

[a] Abbreviations: PPAR, peroxisome proliferator-activated receptor; SPPARM, selective peroxisome proliferator-activated receptor modulator; NR, nuclear receptor; TZDs, thiazolidinediones; LBD, ligand binding domain; RXR, retinoid X receptor; MD, molecular dynamics; FRET, fluorescence resonance energy transfer; HOBT, hydroxybenzotriazole; DIC, *N*,*N*-diisopropylcarbodiimide; RMSF, root-mean-square fluctuation; ED, essential dynamics; ChIP, chromatin immunoprecipitation.

 Published on Web 05/12/2010

helix 12 (H12) in transcriptional regulation of these nuclear receptors. The structures of PPARγ bound to partial agonists show that there are two classes of ligands: those contacting directly H12, spanning from H11 beyond H3, and those showing no direct interaction with H12, spanning from H3 to the β-sheet. For both classes of compounds, the importance of other regions such as H3 and β-sheet is emerging and their stabilization can also affect the transcriptional response.[16−21] Moreover, the recently solved structure of full-length PPARγ−RXR heterodimer demonstrated that the β-sheet region of PPARγ binds directly to the RXR−DNA binding domain.[22] Thus, differential binding of ligands in the region between β-sheet and H3 of PPARγ may also affect transcriptional activity through modulation of its interaction with RXR.

In the present paper, we focused our attention to these regions of PPARγ, particularly to the factors stabilizing H3. In a previous work,[23] we reported a structural study on two enantiomeric ureidofibrate-like derivatives (Figure 1) complexed, respectively, with the PPARγ−LBD.

The *R* enantiomer, ***R*-1**, behaves as a full agonist of PPARγ, whereas the *S* enantiomer, ***S*-1**, is a less potent partial agonist. Comparing the X-ray structures of the two complexes, we argued that the partial agonist behavior of ***S*-1** could be ascribed to a destabilization of the active conformation of H12. We showed that the suboptimal conformation of H12, observed in the PPARγ−***S*-1** complex, is probably due to a steric hindrance between the ethyl group, linked to the asymmetric carbon atom of the ligand, and the crucial residue Q286 of PPARγ, situated on H3.

In another X-ray and molecular dynamics (MD) work, in which we explained at molecular level the different pharmacological profile of the enantiomers of a novel PPARα/γ dual agonist,[24] we confirmed that a differential stabilization of H3 plays an important role in determining the partial agonist character of a ligand. These results prompted us to perform MD simulation studies on the PPARγ−LBD complexed with the two enantiomers ***S*-1** and ***R*-1** to investigate more deeply the role of H3 stabilization in the presence of partial and full agonists. In this regard, we also examined, during the simulation, the distances between the two residues of the charge clamp in the liganded and unliganded forms in order to evaluate if they fit the right values for the recruitment of the coactivators. We also compared the dynamic behavior of PPARγ−LBD with that of PPARα by MD to understand if the importance of the stabilization of H3 in the mechanism of partial agonism is a property of PPARγ or may be extended to PPARα. Furthermore, we investigated how the two enantiomers affect the recruitment of different coregulators to PPARγ by performing fluorescence resonance energy transfer (FRET) and chromatin immunoprecipitation (ChIP) assays and assessed the functional relevance of some of these coregulators in cell-based transcriptional assays. In addition, we clarified the role of Q286, belonging to H3, on the transcriptional activity of the receptor by testing the effect of site-directed mutagenesis of Q286. Molecular modeling was performed to rationalize the activity of the mutants. Finally, we proposed a hypothesis of mechanism of recruitment of coactivators and corepressors induced upon binding of partial agonists.

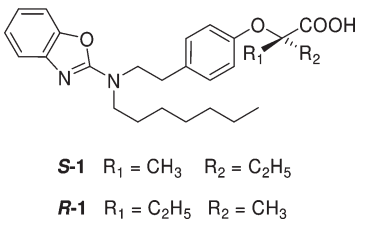

Figure 1. Schematic diagram of ***R*-1** and ***S*-1** enantiomers.

Chemistry

The synthesis of the ***S*-1** isomer is depicted in Scheme 1 and involved the key intermediate acid ***S*-2**, which was prepared from the condensation of 4-bromo-phenol with 2-butanone in the presence of $CHBr_3$ and KOH, followed by fractional crystallization from ethanol of the diastereomeric salts obtained with (*R*)-1-phenylethylamine. The esterification of acid ***S*-2**, followed by condensation with *N*-vinylphthalimide in the presence of $Pd(AcO)_2$, tri-*o*-tolyl-phosphine, and *N*,*N*-diisopropylethylamine in anhydrous CH_3CN provided the intermediate ***S*-3**. The reduction of compound ***S*-3**, which was achieved by hydrogenation at 4 atm in the presence of Wilkinson catalyst, was followed by hydrazinolysis of the phthalimide moiety leading to the amine intermediate, whose condensation with heptanoic acid in the presence of hydroxybenzotriazole (HOBT) and *N*,*N*-diisopropylcarbodiimide (DIC) afforded the intermediate ***S*-4**. The amide group of compound ***S*-4** was reduced with 1 M borane in THF solution to give the corresponding amine. The condensation of this intermediate with 2-chloro-benzoxazole, followed by saponification of the ester function, led to the final acid ***S*-1**. The

Scheme 1. Synthesis of the PPAR Agonist ***S*-1**[a]

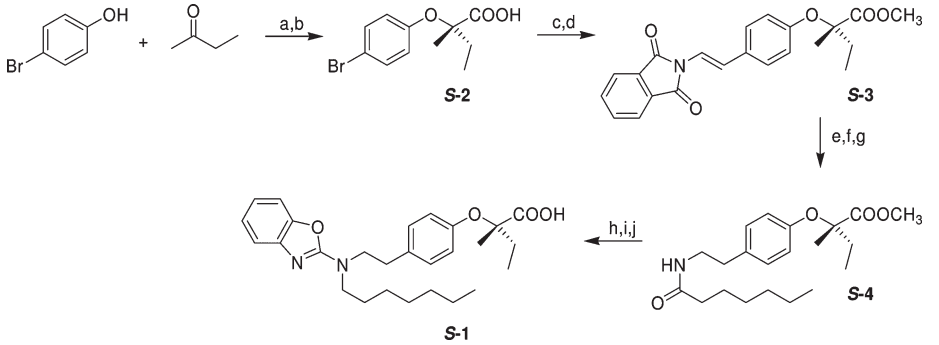

[a] (a) $CHBr_3$, KOH; (b) fractional crystallization from EtOH of the (*R*)-1-phenylethylamine salts; (c) MeOH, H_2SO_4 cat.; (d) *N*-vinylphthalimide, $Pd(AcO)_2$, tri-*o*-tolylphosphine, *N*,*N*-diisopropylethylamine, CH_3CN; (e) H_2 (4 atm), Wilkinson cat., EtOH, rt; (f) $N_2H_4 \cdot xH_2O$, EtOH; (g) heptanoic acid, HOBT, DIC, CH_2Cl_2; (h) 1 M BH_3 in THF; (i) 2-chloro-benzoxazole, $(Et)_3N$, THF; (j) 1 N NaOH, EtOH, rt.

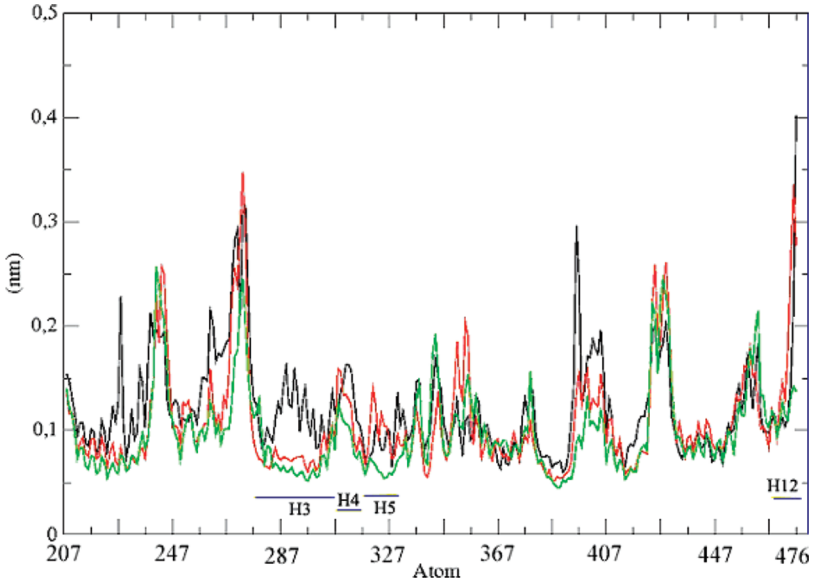

Figure 2. Cα rms fluctuation of apo-PPARγ (black), and PPARγ−***R*-1** (red) and PPARγ−***S*-1** (green) complexes.

Scheme 2. Synthetic Pathway for the Preparation of ***R*-2**

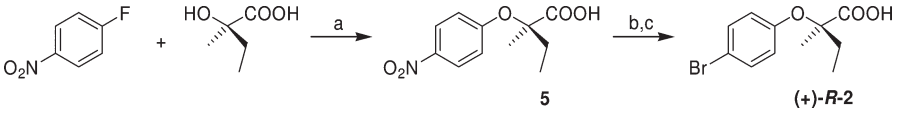

(a) 95% NaH, DMF, reflux; (b) H_2 (4 atm), 10% Pd/C; (c) 48% HBr, $NaNO_2$, CuBr, from 0 to 80 °C.

synthesis of the ***R*-1** isomer was carried out by following the same synthetic pathway described in Scheme 1 starting from compound ***R*-2**. Both enantiomers of acid **1** had enantiomeric excesses >98% as determined by HPLC analysis on chiral stationary phase (see Experimental Section).

The absolute configuration of ***R*-1** and ***S*-1** was determined by chemical correlation by preparing one of the enantiomers of the key intermediate **2** through a synthetic pathway with assigned stereochemistry as depicted in Scheme 2. For this purpose, the *R*-2-hydroxy-2-methyl-butanoic acid, obtained by fractional crystallization of its diastereomeric salts with brucine,[25,26] was condensed with 4-nitro-fluorobenzene to give the 4-nitro-phenoxy intermediate **5** with retention of configuration. The hydrogenation of the nitro group, followed by the treatment with 48% HBr, $NaNO_2$, and CuBr, led to the acid (+)-**2** with the same *R* configuration of the starting α-hydroxy acid.

Results

MD Simulation Analysis. From the analysis of the root-mean-square fluctuation (RMSF) of PPARγ−LBD before (apo-form) and after complexation with the enantiomers ***R*-1** and ***S*-1** (Figure 2), the following main considerations can be drawn: (a) H3 in the apo-form fluctuates to a larger extent with respect to both the complexed forms. (b) H3 stabilization realized by the binding of the ligands is greater in the case of ***S*-1**; although small, the RMSF difference between the two complexes can be considered significant taking into account the maximum error equal to ±0.02 nm evaluated by dividing the overall trajectory in two subportions. Even performing MD simulation starting from an inactive conformation of H12, similar to that adopted in the ternary complex of the antagonist **6** (GW6471, Figure 8) with PPARα and the corepressor SMRT,[27] H3 is less fluctuating in the presence of ***S*-1** than ***R*-1** (Figure 1 of Supporting Information). (c) A comparison between the Cα RMSF analysis of the apo-form of PPARα, performed in a previous work,[24] and that of PPARγ evidences that in PPARα, unlike PPARγ, H3 is stable even in the absence of the ligand (Figure 2 of Supporting Information). (d) The fluctuation of H12 is very high in the apo-form and in the complex with ***R*-1**; on the contrary, H12 results more stabilized upon the binding of ***S*-1**. (e) Helices H4 and H5 are also less fluctuating upon the binding of ***S*-1**.

Table 1. Backbone Atom Traces

apo-PPARγ	backbone = 13.153 nm^2
PPARγ−***R*-1**	backbone = 11.099 nm^2
PPARγ−***S*-1**	backbone = 8.715 nm^2

Analysis of the Trajectories. A better view of dynamical−mechanical properties of the investigated system has been obtained by using essential dynamics (ED) analysis.[28] This procedure is based on the construction of the backbone covariance matrix whose trace, reported in Table 1, quantitatively provides the fluctuation pattern of the system. Our results clearly indicate that ***S*-1** stabilizes PPARγ−LBD more than ***R*-1**.

At the same time, the diagonalization of the covariance matrix also provides the set of eigenvectors along which the system fluctuates and the extent of the fluctuation. The spectrum of the corresponding eigenvalues (Figure 3 of Supporting Information) indicates that the fluctuation of the system is basically confined within the first two eigenvectors. The 2D projection of the trajectories onto the first two apo-form eigenvectors shows that the binding of the two enantiomers (red and green points in Figure 3) dramatically changes the configurational space sampled by the complexed

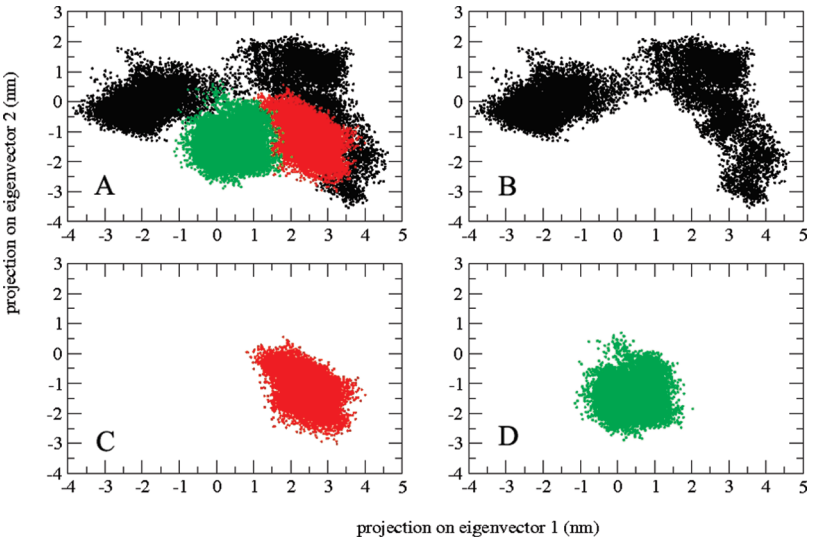

Figure 3. Trajectory projection on the first two eigenvectors of (A) apo-PPARγ (black dots) and of PPARγ complexed with the full agonist ***R*-1** (red dots) and the partial agonist ***S*-1** (green dots). For clarity's sake, each trajectory projection is also shown separately in (B−D).

PPARγ−LBD with respect to that of the apo-LBD (black points).

Interestingly, while the more restricted area sampled by the ***R*-1** complexed form is inside the extended area of the apo-form, that one sampled by the ***S*-1** complexed form lies in a new region, outside the region of the apo-form. In other words, the presence of ***R*-1** induces mechanical−dynamical alterations of the LBD backbone to a lower extent with respect to ***S*-1**.

The Charge Clamp. We analyzed the average distance between the Cα atoms of the residues K301 and E471, the two residues constituting the so-called "charge clamp", during the 15 ns of the simulation. The correct positioning of these two charged residues is very important for the recruitment of the coactivator, allowing the right orientation of the two-turn helix dipole of the coactivator in the hydrophobic cleft of the nuclear receptor. We found that the average distance between the two residues is 19.0 Å in the apo-form, 17.7 Å in the ***R*-1** complex, and only 17.3 Å in the ***S*-1** complex. The standard errors are below 0.01 Å.

Interaction of PPARγ with Coregulators in the Presence of Rosiglitazone, *R*-1 and *S*-1. We next analyzed the functional consequences of ***R*-1** and ***S*-1** binding on the capacity of PPARγ to associate with coregulators. For this purpose, we performed FRET assays with a panel of biotinylated peptides for the coregulators SRC-1, PGC-1α, RIP140, CBP, TIF-2, and N-CoR1 in the presence of saturating concentrations of the ligands and increasing amounts of the peptides. Under these conditions, we could evaluate the affinity of PPARγ, activated by ***R*-1**, ***S*-1**, or rosiglitazone, for each coregulator (Table 2). As shown in Figure 4, in the presence of the ligands all the tested coactivators interact with PPARγ with similar EC_{50}, except CBP (NR box 1) whose affinity is higher with rosiglitazone (Table 2). This might explain, at least in part, the higher potency of rosiglitazone as compared to that of ***R*-1** and ***S*-1** observed in cell-based transcription assays.[23] Notably, the most striking difference is the association of the corepressor N-CoR1 in the presence of ***S*-1** as opposed to rosiglitazone and ***R*-1**, providing an explanation to our previous observations whereby ***S*-1** is a partial agonist, whereas the *R* enantiomer is a full agonist of PPARγ.[23] In this case, the amount of N-CoR1 associated to PPARγ is comparable to that of the unliganded receptor. We did not detect any interaction between PPARγ and the corepressor SMRT in FRET assay in all tested conditions (data not shown). We finally tested two alternative peptides for the coregulators CBP (NR box 4) and RIP140 (NR box 7). CBP (NR box 4) does not show association (data not shown), whereas RIP140 (NR box 7) can interact with PPARγ (Figure 4 of Supporting Information) although the EC_{50} in this case is higher, indicating that this region of RIP140 poorly interacts with the receptor.

Table 2. EC_{50} Values of Peptides Recruited to PPARγ in the Presence of Saturating Concentrations of Rosiglitazone (10 μM), ***R*-1** (25 μM), and ***S*-1** (50 μM)[a]

	EC_{50} (μM)		
coregulator peptide	rosiglitazone	***R*-1**	***S*-1**
SRC-1 (NR box 2)	2.0435 ± 0.012	2.37 ± 0.245	3.6155 ± 0.652
PGC-1α (NR box 1)	0.36 ± 0.075	0.3206 ± 0.055	0.4223 ± 0.078
RIP140 (NR box 4)	0.2676 ± 0.041	0.2408 ± 0.051	0.3319 ± 0.061
RIP140 (NR box 7)	0.88495 ± 0.296	1.0454 ± 0.207	1.0655 ± 0.043
CBP (NR box 1)	0.091 ± 0.004	0.1801 ± 0.054	0.1715 ± 0.019
TIF2 (NR box 2)	0.7996 ± 0.057	0.9132 ± 0.191	1.736 ± 0.414
N-CoR1 (NR box 1)	> 100	> 100	0.8134 ± 0.073

[a] Values are mean ± SE.

Recruitment of N-CoR1 on the Promoters of PPARγ Target Genes. To assess the relevance of the association of N-CoR1 to PPARγ in the presence of ***S*-1**, we next performed ChIP experiments examining the corepressor occupancy on the promoter of the lipoprotein lipase (LPL) and of the scavenger receptor CD36 genes, two known PPARγ targets in RAW264.7 cells. The results show that N-CoR1 is recruited on the PPRE of both LPL and CD36 promoters in control cells and, at a greater extent, in the presence of the PPARγ antagonist **7** (GW9662, Figure 5).[29] More interestingly, the corepressor is still associated to the promoters in the presence of ***S*-1**, whereas the treatments with rosiglitazone or ***R*-1** significantly reduce the recruitment of N-CoR1, as expected. These observations further indicate that the partial agonist behavior of ***S*-1** could be due to the particular conformation adopted by PPARγ that does not allow the release of the corepressor at the extent observed with full agonists. The specificity of N-CoR1 recruitment on target

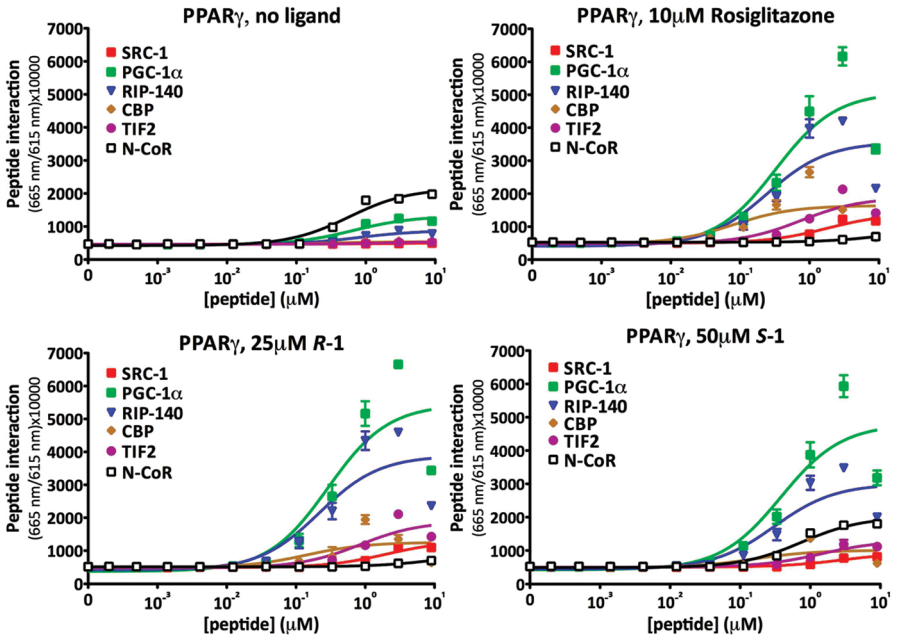

Figure 4. Coregulator interaction with PPARγ by FRET assays. The association of six different coregulators SRC-1, PGC-1α, RIP140, CBP, TIF-2, and N-CoR1 to PPARγ in the presence of 10 μM rosiglitazone, 25 μM ***R*-1** and 50 μM ***S*-1** was studied by FRET assays, using increasing concentrations of the indicated biotinylated peptides. The curves are expressed as the ratio of fluorescence reading at 665 and 615 nm multiplied by 10000 and represent the mean ± SE of independent curves.

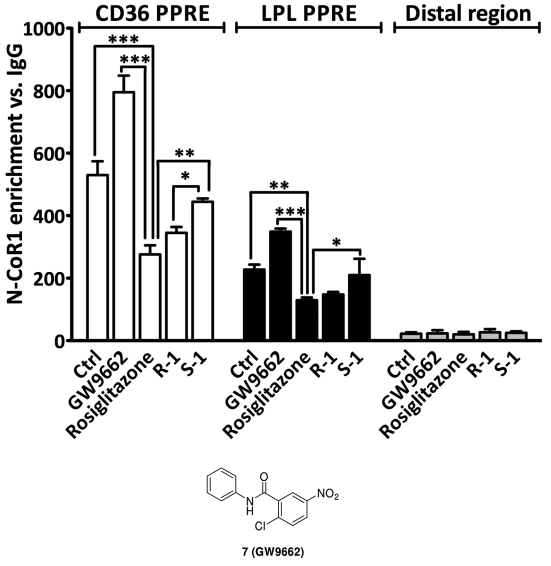

Figure 5. N-CoR1 recruitment to PPARγ target gene promoters by ChIP assay. RAW264.7 cells were treated with 5 μM PPARγ antagonist **7** or 5 μM rosiglitazone or 5 μM ***S*-1** or 5 μM ***R*-1** for 16 h. ChIP assay was performed with antibody against N-CoR1 or control IgG. Immunoprecipitated DNA was analyzed by real time PCR using primers specific for the PPREs of CD36 and LPL promoters or for a distal region as a negative control. Results are expressed as mean ± standard deviations of triplicate samples. Statistical significant differences were assessed by one-way ANOVA with Tukey's post test. (*), (**), (***) indicate $P < 0.05$, $P < 0.01$, $P < 0.001$, respectively.

PPRE was confirmed by evaluating its association with a distal genomic region.

Role of Coregulators on PPARγ Activity. We next determined the functional relevance of the coregulator interaction with PPARγ observed in FRET assays in a cellular context. To this end, we cotransfected cells with Gal4−PPARγ−LBD expression vector with a panel of different coregulators (PGC-1α, CBP, RIP140, and N-CoR1) along with the luciferase reporter gene under the control of Gal4 binding sites. As shown in Figure 6, PGC-1α enhances both the basal and the induced transcription activity of Gal4−PPARγ in the presence of all tested ligands about 3-fold as compared to cells with no overexpressed coregulator (compare activity of wt constructs in panel A vs B of Figure 6). The overexpression of CBP gives a similar pattern (compare activity of wt constructs in panel A vs C of Figure 6). When RIP140 was overexpressed, the basal activity was not affected, however the stimulation of all ligands was blunted (compare activity of wt constructs in panel A vs D of Figure 6), suggesting that this coregulator behaves as a repressor. Finally, the corepressor N-CoR1 leads to decreased basal activity of Gal4−PPARγ, while in the presence of rosiglitazone and ***R*-1** we observed a clear stimulation of the receptor activity, but ***S*-1** modestly affected the transcriptional activity (compare activity of wt constructs in panel A vs E in Figure 6).

Mutagenesis of the Q286 Residue of PPARγ. To validate the functional relevance of the residue Q286 that is involved in the steric hindrance with ***S*-1**,[23] we substituted this residue with amino acids bearing side chains of different length and polarity. In particular, the following mutants have been generated: Q286A, Q286D, Q286E, Q286K, and Q286M (Figure 6). The substitution Q286A reduces the basal activity of PPARγ and, to a lower extent, the activity in the presence of rosiglitazone and ***R*-1**. Conversely, ***S*-1** is ineffective on the Q286A mutant, suggesting that with this amino acid substitution the *S* enantiomer does not induce a conformational change of the receptor favorable for its activation. When Q286 was mutated to an acidic amino acid, we obtained different behaviors as compared to the wild type receptor. The basal activity of Q286D mutant decreases, whereas that of Q286E improves very strongly (4-fold with respect to that of the wild type). The activity of the mutant Q286D is virtually unaffected by the ligands. No ligand can also increase the activity of the Q286E mutant, indicating that

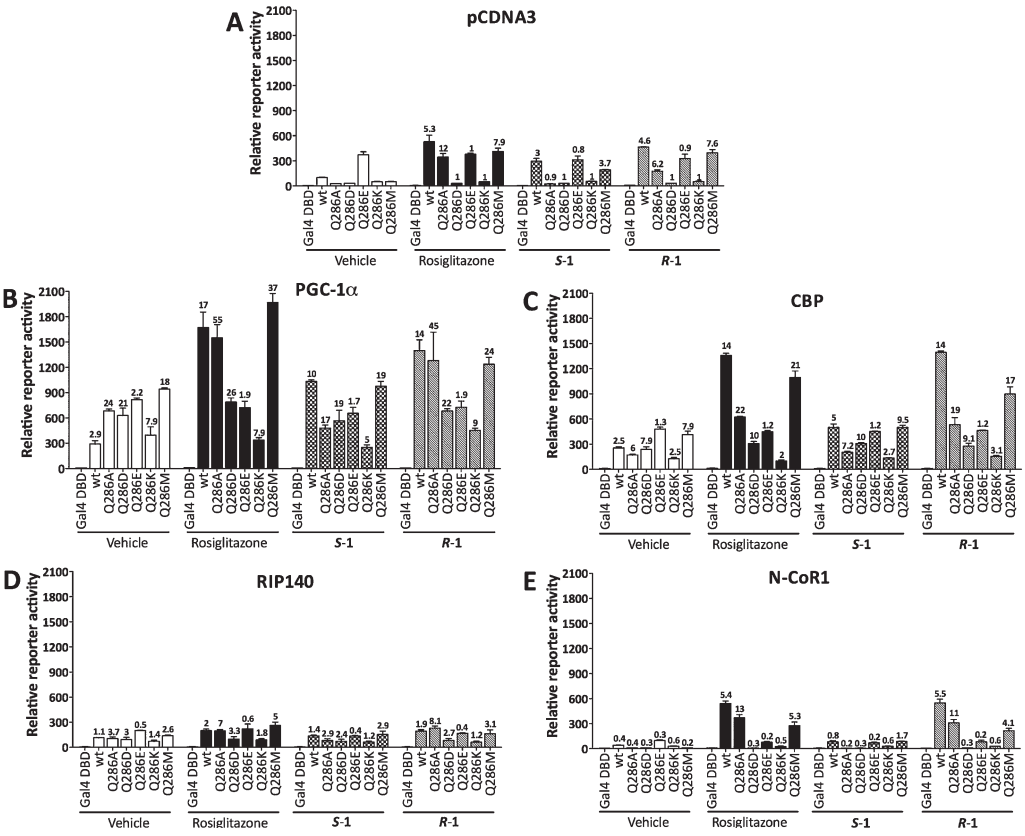

Figure 6. Effect of coregulators on the transcriptional activity of PPARγ and analysis of point mutants. The effect of the overexpression of the coregulators PGC-1α (B), CBP (C), RIP140 (D), and N-CoR1 (E) on the basal and ligand-stimulated transcription activity of PPARγ was tested in cotransfection assays in HEK293 cells. Rosiglitazone, ***S*-1**, and ***R*-1** were added at a final concentration of 5 μM in dimethyl sulfoxide (DMSO). The effect of the same coregulators in the absence and in the presence of ligands was also tested on the transcriptional activity of the indicated mutants of PPARγ. Results are expressed as percentage of wt in the absence of ligands, and each point is the mean ± SE of three independent experiments each performed in triplicate wells. The fold activation of each mutant as compared with the vehicle (DMSO) is indicated above the bars.

the introduction of a glutamate residue in this position may lock the apo-receptor in the active conformation and the addition of ligands cannot increase the transcription activity any further. When a lysine residue substituted for Q286, the basal receptor activity dropped dramatically and cannot be restored by ligands. Finally, the substitution Q286M reduces the basal activity and, to a lower extent, the activity in the presence of rosiglitazone and ***R*-1**. Notably, ***S*-1** affects the transcriptional activity of PPARγ Q286M to a lesser extent as opposed to rosiglitazone and ***R*-1**. Interestingly, PGC-1α and CBP increase both the basal and ligand-dependent transcription activity of mutant Gal4−PPARγ, thus overcoming the defective activity of the mutant forms of the receptor (Figure 6A,B,C). On the other hand, RIP140 improves the basal activity of the mutants to the level of that of the wt, with the exception of Q286E mutant, which is reduced; instead, this coregulator dampens the ligand-dependent transcription activity of the mutated receptors (Figure 6A,D). The overexpression of the corepressor N-CoR1 determines a general reduction of the activities of all the mutated forms of Gal4−PPARγ in the presence of all tested ligands (Figure 6A,E), except for the mutant Q286A in the presence of rosiglitazone and ***R*-1**, underlying the importance of the glutamine residue in determining the behavior of ***S*-1**.

Discussion

The essential dynamics traces of PPARγ−LBD with and without the ligands show a global stabilization of the liganded forms with respect to the apo-form, but unexpectedly, the ***S*-1** ligand, which behaves as a partial agonist, seems to better stabilize the PPARγ−LBD compared to the full agonist ***R*-1** (8.7 nm^2 vs 11.1 nm^2). The analysis of the 2D projection of trajectory on the two essential eigenvectors demonstrates that the configurational space sampled by the ***S*-1** complex during the simulation lies on a different region from that of the apo-form and the ***R*-1** complexed form (Figure 3). The complex with the full agonist ***R*-1** lies in a restricted area of the configurational space, which is inside the extended area of the apo-form. This common region would correspond to a population of active conformations able to recruit coactivators. The conformationally mobile apo-PPARγ−LBD could also assume, in fact, active conformations, as evidenced by its rather high basal activity.[30] It is conceivable to suppose that the different region covered by the complex with the partial agonist ***S*-1** represents a population of LBD conformations more stable compared to ***R*-1** but less productive for the coactivator recruitment. In fact, the EC_{50} values relative to the interaction of the coactivators SRC-1, PGC-1α, and TIF2 are slightly higher in the complex with ***S*-1** compared to ***R*-1** (Table 2), indicating that the affinity for these coactivators decreases with the partial agonist. Looking at the RMSF analysis, it is evident that ***S*-1** better stabilizes H3 and H12 with respect to ***R*-1**. These results confirm the hypothesis, already advanced by our previous X-ray studies on these two enantiomers, that the partial agonist ***S*-1** is not able to stabilize H12 in the proper position to efficaciously recruit the

Table 3. Cα Distances between K301 and E471 in the Ternary Complexes of PPARγ with Ligands and SRC-1 Coactivator Fragment[a]

PDB code	Å
1FM9	19.6
1K74	19.9
2PRG	18.7, 19.6[a]
1FM6	19.6, 19.6[a]

[a] These distances are referred to the two molecules of PPARγ in the asymmetric unit.

coactivator and stabilizes instead a suboptimal conformation of H12, resulting in an attenuated transcriptional response. However, the most striking result observed in our FRET and ChIP analyses is that the corepressor N-CoR1 remains associated to PPARγ in the complex with ***S*-1** at levels comparable to that of samples with no added ligand, suggesting that the conformation adopted by the receptor in the complex with ***S*-1** does not allow the complete release of the corepressor, as observed with the full agonists rosiglitazone and ***R*-1**. Moreover, as shown in the cotransfection assays, when N-CoR1 is overexpressed, the treatment with ***S*-1** fails to induce the transcriptional activity of the wt and mutated Gal4−PPARγ. Therefore, on the basis of these multiple approaches, we propose that the retention of the corepressor bound to PPARγ might be the main explanation for the partial agonist behavior of ***S*-1** as in the case of other partial agonists described for the liver X receptor (LXR).[31,32] Our data indicate that RIP140 and N-CoR1 are corepressors of PPARγ. However, the repressor activity of these two coregulators seems to occur via two different modalities. On one hand, N-CoR1 is constitutively associated to PPARγ in the absence of agonists or even in the presence of the partial agonist ***S*-1**. Full agonists like rosiglitazone and ***R*-1** release N-CoR1 and allow the full activation of the receptor, whereas in the presence of the partial agonist ***S*-1** N-CoR1 is still associated to the receptor and prevents its full activation. On the other hand, the association of RIP140 with PPARγ increases in the presence of ligands and reduces the activity of Gal4−PPARγ, thus suggesting a repressive role of this coregulator on PPARγ as already reported by others.[33] We also confirmed the hypothesis advanced by H/D exchange experiments[18] whereby partial agonists differentially stabilize other regions of the binding pocket. Particularly, the partial agonists of the first class, spanning from H11 and H12 beyond H3, show decreasing efficacy with an increasing stabilization of H3. The compounds of this class preferentially stabilize H3 through H-bonds or closer hydrophobic contacts made with residues of this helix, as in the case of ***S*-1** with the Q286 residue of H3 in PPARγ. This differential stabilization of regions away from H12 suggests that these regions could be involved in the interaction with the coactivators, and this interaction could be mediated by the presence of partial agonists. For example, the CBP coactivator utilizes a more extensive motif than the canonical LxxLL in interacting with the LBD of nuclear receptors, suggesting a binding mode governed by LxxLL motif but modulated by flanking residues and possibly fine-tuned by additional interactions with partial agonists.[34]

In addition, the analysis of average distances between the two residues of the charge clamp shows a deviation, in the case of the complex with the partial agonist ***S*-1** (17.3 Å), from the distance normally observed in the structures of the ternary complexes of PPARγ with the ligand and coactivator motif.[35] It is well-known that in PPARs, as well as in other NRs, the distance between the Cα atoms of these two residues ranges between 18 and 20 Å in the presence of a coactivator and an agonist ligand (Table 3). In the complex with ***R*-1**, this distance is almost within this range (17.7 Å). The hydrophobic cleft for the recruitment of the coactivator is formed by helices 3, 4, and 12 (Figure 7). In the complex with ***S*-1**, the observed short average distance between the residues involved in the charge clamp is probably due to the lower fluctuation of these three helices upon the ***S*-1** binding, representing additional evidence corroborating the hypothesis of a receptor adopting a nonoptimal conformation for the binding of coactivators. Therefore, it is conceivable to suppose that partial agonists like ***S*-1** preferentially select suboptimal less active conformations of the PPARγ−LBD among those possible existing in solution, resulting in a slightly decreased affinity for certain coactivators and do not allow the complete dissociation of corepressors from the receptor.

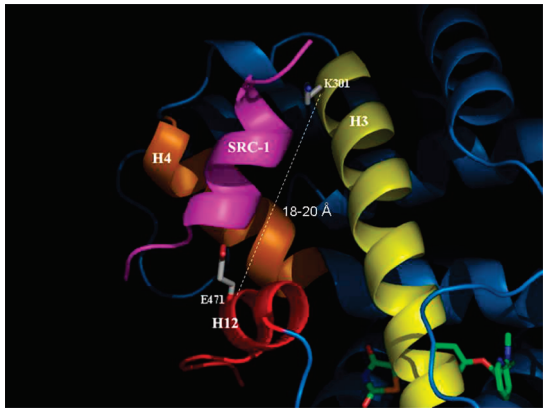

Figure 7. PPARγ coactivator binding surface. The two residues forming the charge clamp are shown in white. The SRC-1 coactivator motif is shown in purple.

Could *S*-1 Be a Selective PPARγ Modulator? The analysis of the EC_{50} values of coregulator recruitment (Table 2) shows that rosiglitazone and ***R*-1** have typical profiles of full agonists and that ***R*-1** behaves in a very similar way to rosiglitazone, recruiting all the tested coactivators almost with the same affinity. Yet, a difference in the EC_{50} value of CBP is observed with ***R*-1** versus rosiglitazone. It is possible that the higher EC_{50} for this coactivator may explain the lower potency of this enantiomer as compared to rosiglitazone. The partial agonist ***S*-1** shows a more interesting profile of interaction with coregulators. With this ligand, the EC_{50} values of all coactivators are higher, in particular that of CBP and TIF-2, with respect to that obtained with rosiglitazone. Most strikingly, however, ***S*-1** is able, unlike the other two ligands, to recruit the corepressor N-CoR1, providing a functional explanation to the partial agonist behavior of this ligand. As demonstrated in the only known crystal complex with a corepressor, the ternary complex PPARα−SMRT−**6**[27] (Figure 8), when the corepressor is bound to PPAR−LBD its three-turn α-helix extends into the space normally occupied by the active conformation of H12. This helix, displaced by the antagonist, is repositioned toward H3 and it is loosely packed against it. In this way, the corepressor is bound into the hydrophobic cleft formed by H3, H4, and H12, with the last one forming a different edge of the hydrophobic cleft compared to the complex with the coactivator. The behavior of ***S*-1** suggests that this ligand is able to stabilize the H12 for recruiting the coactivators, although in a suboptimal way. This is evidenced in the crystal structure of PPARγ−***S*-1**[23] and

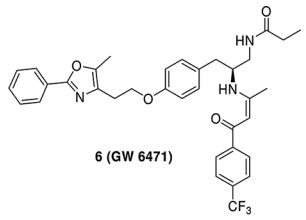

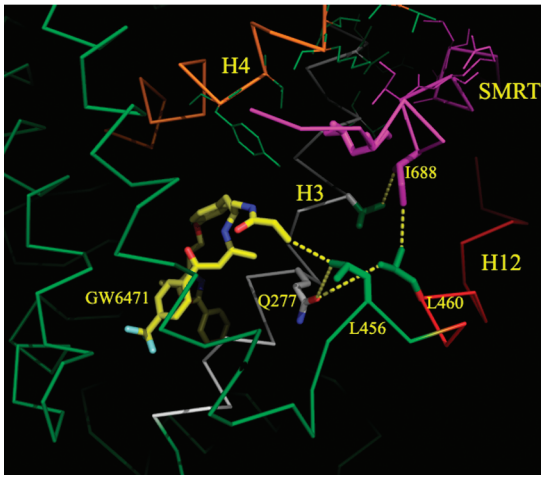

Figure 8. The ternary complex of PPARα−SMRT−**6** (PDB code 1KKQ). The ligand is shown in yellow, the corepressor SMRT in pink, H12 in red, H4 in orange, and H3 in white; the residue Q277 is also shown in white.

in our MD simulations which show a nonoptimal distance between the residues forming the charge clamp. At the same time, ***S*-1** would be also able to stabilize H3 and H4, as demonstrated by the MD simulations, in such a way to allow, alternatively, the accommodation of the corepressor upon rearrangement of H12 against H3. As shown in Figure 8, in fact, the corepressor is held in its position through several interactions with H3 and H4, hence a better stabilization of these helices by a partial agonist like ***S*-1** turns out to be very important for the recruitment of the corepressor and also for the stabilization of H12 in its inactive conformation close to H3. In this regard, we performed a further MD simulation, with ***R*-1** and ***S*-1**, starting from an inactive conformation of H12, similar to that assumed in the ternary complex PPARα−SMRT−**6**. As shown in Figure 1 of Supporting Information, also in this case H3 is less fluctuating in the presence of ***S*-1**, indicating that its greater stability does not depend on H12 conformation but only on the ligand. Moreover, the stabilization of H3 seems to favor the inactive conformation of H12 and also of the loop 11/12, as indicated by the lower RMSF of these regions when ***S*-1** is present (see Figure 1 of Supporting Information), helping in this way the recruitment of corepressor or diminishing its release. All these observations are corroborated by both FRET analysis with coregulator peptides and ChIP assays, the latter providing a snapshot of the actual association of the corepressor N-CoR1 with PPARγ in the presence of the partial agonist ***S*-1**.

The behavior of ***S*-1** at molecular level, therefore, seems to account for its PPARγ partial agonism and makes it a good candidate as a selective modulator, that is, a molecule able to function as a full agonist in some tissues where a sufficient amount of coactivators is available and as a partial agonist or antagonist in specific tissues with different ratio of coactivator/corepressor proteins.

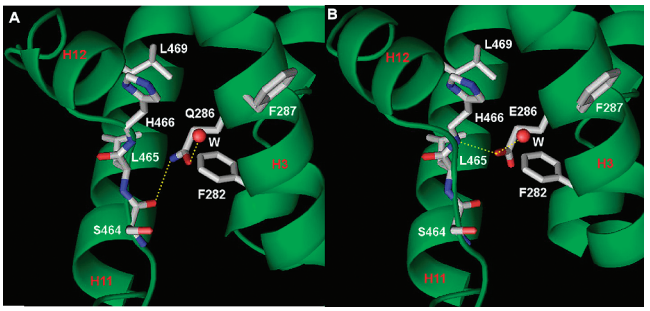

Figure 9. Main interactions of Q286 into the apo-form of wt PPARγ (A) and of E286 into the mutant Q286E (B).

The Key Role of Q286. In Figure 8, it is also possible to notice the key role of the residue Q277 of PPARα (equivalent to Q286 in PPARγ) in stabilizing H12 in its inactive conformation. On the other hand, as previously reported,[23] this residue was demonstrated to play a determinant role even in the stabilization of the active conformation of H12. These observations strengthened further our project to carry out a site-directed mutagenesis of Q286 in PPARγ. The mutation analysis made on this residue clearly evidence its key position in H3 for the stabilization of H12, in some cases also in the absence of the ligand. As can be seen in Figure 9A, in the apo-form of wild type PPARγ, the residue Q286 is involved in two H-bonds: the former between the CO group and a crystal water molecule and the latter between the NH_2 group and the CO of S464 belonging to the loop 11/12. Upon the binding of rosiglitazone[36] or ***R*-1**[23] and, to a lesser extent, of ***S*-1**,[23] a network of strong interactions can be realized among the ligand, H3, and the loop 11/12. These interactions stabilize the active conformation of H12 better than in the apo-form. In this network, Q286 plays a crucial role through its $CONH_2$ group. In the PPARγ−rosiglitazone complex, the NH_2 group makes a H-bond with a CO of the ligand thiazolidinedione ring and an amino-aromatic interaction with F282, while the CO group engages a H-bond with a crystal water, which bridges in turn the backbone NH of H466 (loop 11/12). ***S*-1** and ***R*-1** complexes with PPARγ are stabilized by two H-bonds, a stronger one between Q286 NH_2 and S464 backbone CO and a weaker one between Q286 CO and H466 backbone NH.

To seek structural explanations for the effects of Q286 substitutions in PPARγ, we used molecular modeling to assess how these mutations would affect both receptor basal activity and ligand binding. Using the Rotamer Explorer function[37] inside MOE,[38] Q286 was computationally mutated in the ligand-free PPARγ (PDB code 1PRG)[36] and in rosiglitazone (PDB code 2PRG),[36] ***S*-1** (PDB code 2I4P),[23] and ***R*-1**-bound (PDB code 2I4J)[23] structures, and the most favorable rotamers of each residue were examined. These rotamers were determined based on the lowest ΔG. ΔG is the sum of the change in free energy of solvation between the states where protein and rotamer are separated and when they form a complex plus the torsional strain of the rotamer.

Figure 6 shows the effect of the mutation of Q286 on the transcriptional activity. The basal activity of all the mutants, with the only exception of Q286E, is reduced. The basal activity of the mutated forms of PPARγ can be restored only if supraphysiological levels of coactivators are present in the cells, as in the case of cotransfected PGC-1α and CBP. Intriguingly, we observed that RIP140 reduces the basal activity of the Q286E mutant, which is otherwise strongly

enhanced, thus further supporting its role as a corepressor. The reduced basal activity of the mutants could be explained by the loss of the H-bond made by Q286 with the carbonyl oxygen of S464. None of the mutants has functional groups able to make this H-bond, with the exception of Q286D and Q286E. Nevertheless, D has a shorter side-chain with respect to Q and cannot form H-bonds with the backbone of the loop 11/12. On the contrary, the side-chain of E, equal in size to Q, is able to form a charge-reinforced H-bond with the backbone NH of H466 (Figure 9B). This would account for a strong interaction between H3 and the loop 11/12, up to the beginning of H12, able to stabilize this helix also in the absence of a ligand. This network of interactions would be efficient to such an extent that the binding of a ligand would not affect at all the activity. Looking at activities in the presence of the ligands, it is evident that ***S*-1** does not affect the mutants activities but only that of the wild type receptor (6.4-fold the basal activity) and, to a lesser extent, that of Q286M (3.1-fold). On the contrary, ***R*-1** and rosiglitazone improve the activity of the hydrophobic mutants Q286A and Q286M possessing a terminal methyl group which can interact with the ligands through vdW contacts, partially restoring the activity of the wild type receptor (Figures 5A−B and 6A−B of Supporting Information). The activity of the mutants Q286K and Q286D is impaired also in the presence of the ligands. Particularly, the long and positively charged side-chain of lysine adopts a low-energy *trans*−*gauche* conformation which prevents any local interaction with the protein, thus destabilizing the loop 11/12 (Figure 7 of Supporting Information).

Conclusions

The behavior of the ligand ***S*-1** allows one to suppose that some PPARγ partial agonists would be able to select populations of the LBD with nonoptimal distances between the residues of the charge clamp. This could allow the stabilization of suboptimal active conformations of H12 which would be still able to recruit the coactivator, even though with reduced affinity. At the same time, the suboptimal conformation of H12 could favor its repositioning toward H3 assuming, in this way, a nonactive conformation able to recruit the corepressor, as observed in the ternary crystal complex PPARα−SMRT−**6**. This recruitment could be further enhanced by the better stabilization of H3 and H4 induced by ***S*-1**. In other words, in the presence of partial agonists like ***S*-1**, H12 could function as a switch; its active conformation, although suboptimal, would allow the recruitment of coactivators, whereas its inactive conformation against H3 could favor the binding of corepressors.

This behavior, moreover, seems to be characteristic of PPARγ and not of PPARα. Therefore, the capability to induce both the recruitment of coactivators and corepressors makes ***S*-1** a good candidate as a selective PPARγ modulator, namely a ligand that, depending on the balance between coactivators and corepressor in a given tissue, could behave as an agonist or antagonist. In fact, the cotransfection experiments confirm that when N-CoR1 is overexpressed, ***S*-1** behaves almost like an antagonist, whereas ***R*-1** and rosiglitazone can activate the receptor activity, being a full agonist of PPARγ.

By site-directed mutagenesis, we also confirmed, as previously reported, the crucial role of the residue Q286 in the stabilization of H12 of PPARγ. In addition, the mutation analysis showed that one mutant of this residue is able to directly stabilize H12 also in the absence of a ligand, giving rise to improved basal activity. The strategic position of Q286 in H3 is also highlighted by the fact that only the two potent full agonists rosiglitazone and ***R*-1** are still able to activate the receptor after the mutation of this residue, whereas the less potent partial agonist ***S*-1** turns out to be practically ineffective.

Experimental Section

Chemical Methods. Column chromatography was performed on ICN silica gel 60 Å (63−200 μm) as a stationary phase. Melting points were determined in open capillaries on a Gallenkamp electrothermal apparatus and are uncorrected. Mass spectra were recorded with a HP GC/MS 6890−5973 MSD spectrometer, electron impact 70 eV, equipped with HP chemstation. For GC/MS analysis of acid analytes, the corresponding methyl esters, obtained by reaction with a solution of diazomethane in Et_2O, were used. ^1H NMR spectra were recorded in $CDCl_3$ on a Varian-Mercury 300 (300 MHz) spectrometer at room temperature (20 °C). Chemical shifts are expressed as parts per million (δ). Purity of all tested compounds was >95%, as confirmed by combustion analysis carried out with an Eurovector Euro EA 3000 model analyzer. Optical rotations were measured with a Perkin-Elmer 341 polarimeter at room temperature (20 °C): concentrations are expressed as g(100 mL)$^{-1}$. The enantiomeric excesses of the final acids were determined by HPLC analysis on Chiralcel OD column (4.6 mm i.d. × 250 mm, Daicel Chemical Industries, Ltd., Tokyo, Japan). Analytical liquid chromatography was performed on a PE chromatograph equipped with a Rheodyne 7725i model injector, a 785A model UV/vis detector, a series 200 model pump, and a NCI 900 model interface. Chemicals were obtained from Aldrich (Milan, Italy), Lancaster (Milan, Italy), or Acros (Milan, Italy) and were used without any further purification.

Preparation of (+)-*R*- or (−)-*S*-2-(4-Bromo-phenoxy)-2-methyl Butanoic Acid (*R*-2 and *S*-2). A solution of KOH (29.21 g, 52.11 mmol) in H_2O (75 mL) was added dropwise to a solution of 4-bromo-phenol (15.1 g, 86.78 mmol) in 2-butanone (130 mL). After 0.5 h at room temperature, a first amount of $CHBr_3$ (5.5 mL) was added dropwise, during 1 h, to the reaction mixture. After 1 h at room temperature, a second addition of $CHBr_3$ (11.5 mL) was carried out during 1.5 h. The resulting mixture was stirred overnight at room temperature, after which the organic solvent was distilled off. The aqueous phase was carefully acidified with 6 N HCl and extracted with ethyl acetate. The collected organic phase was washed with brine, dried over Na_2SO_4, filtered, and evaporated to dryness affording a brown oily residue, which was dissolved in ethyl acetate and extracted five times with $NaHCO_3$ saturated solution. The aqueous phase was carefully acidified with 6 N HCl and extracted four times with Et_2O. The collected organic layer was dried over Na_2SO_4, filtered, and evaporated to dryness to give a dark-red oily residue, which was chromatographed on a silica gel column (petroleum ether/ethyl acetate/MeOH 7:2:1 as eluent), affording the desired acid **2** as a pale-yellow solid in 75% yield.

Both enantiomers of **2** were obtained by fractional crystallization of the diastereomeric salts with the chiral resolving agent *S*- or *R*-1-phenylethylamine. For this purpose, a solution of *R*-1-phenylethylamine (10.6 g; 87 mmol) in absolute EtOH (15 mL) was added to a solution of the racemic acid (21.6 g; 79.1 mmol) in absolute EtOH (30 mL). The resulting mixture was stirred for 1 h at 40 °C. The EtOH was distilled off, affording a white solid mixture of the two diastereomeric salts, which was recrystallized from ethyl acetate until the $[\alpha]_D$ had reached a constant value ($[\alpha]_D = -8.3$, *c* 2, MeOH).

The optically pure diastereomeric salt, obtained after six recrystallizations, was suspended in Et_2O (20 mL) and 6 N HCl (15 mL) was added to the suspension. The resulting mixture was stirred for 0.5 h at room temperature, and the organic layer was separated, washed with brine, and dried over Na_2SO_4. The

organic solvent was evaporated to dryness, affording the title acid (−)-***S*-2** (1.51 g; 5.35 mmol) as a colorless oil. (+)-***R*-2** was obtained following the procedure described above using *S*-1-phenylethylamine as a chiral resolving agent.

Preparation of (+)-*R*- or (−)-*S*-Methyl 2-(4-Bromo-phenoxy)-2-methylbutanoate (Step c, Scheme 1). A solution of acid ***R*-** or ***S*-2** (10 mmol) in MeOH (40 mL) and two drops of conc H_2SO_4 was stirred for 3 h at reflux, and then the solvent was distilled off and the residue was dissolved in ethyl acetate. The resulting solution was washed with $NaHCO_3$ saturated solution and brine, and then the organic phase was dried over Na_2SO_4 and the solvent was removed under reduced pressure to give the title compounds as pale-yellow oils.

Preparation of *R*- or *S*-Methyl 2-[4-(2-Phthalimido-2-yl-ethen)-phenoxy]-2-methylbutanoate (*R*-3, *S*-3). A solution of *R*- or *S*-methyl 2-(4-bromo-phenoxy)-2-methylbutanoate (6.19 mmol), tri-*o*-tolyl-phosphine (0.48 mmol), *N*-vinylphthalimide (6.19 mmol), and *N*,*N*-diisopropylethylamine (9.27 mmol) in anhydrous CH_3CN (12 mL) was added, under N_2 atmosphere, to a suspension of $Pd(AcO)_2$ (0.16 mmol) in the same anhydrous solvent (2 mL). The reaction mixture was stirred for 24 h at reflux, and then the organic solvent was evaporated in vacuo and CH_2Cl_2 (20 mL) was added to the residue. The precipitate was filtered off through a celite pad, washed four times with CH_2Cl_2 (20 mL), and the filtrate was washed with brine and dried over Na_2SO_4. The solvent was evaporated to dryness affording a yellow solid residue, which was chromatographed on a silica gel column (petroleum ether/ethyl acetate 9:1 as eluent) to give the title compound as a yellow solid, which was used in the next step without any further purification.

Preparation of *R*- or *S*-Methyl 2-[4-(2-Phthalimido-2-yl-ethyl)phenoxy]-2-methylbutanoate (Step e, Scheme 1). A solution of ***R*-3** or ***S*-3** (5.82 mmol) in THF (35 mL) was added to a stirred suspension of Wilkinson catalyst (350 mg, 0.38 mmol) in abs EtOH (5 mL). The resulting mixture was stirred at room temperature under H_2 atmosphere (4 atm) for 5 h. The suspension was filtered through a celite pad to remove the catalyst, and the solvent was evaporated to dryness, providing a dark solid residue which was chromatographed on a silica gel column (petroleum ether/ethyl acetate 7:3 as eluent), affording the desired compound as a yellow solid.

Preparation of *R*- or *S*-Methyl 2-[4-(2-Amino-ethyl)phenoxy]-2-methylbutanoate (Step f, Scheme 1). $N_2H_4 \cdot xH_2O$ (31.50 mmol) was added to a solution of *R*- or *S*-methyl 2-[4-(2-phthalimido-2-yl-ethyl)phenoxy]-2-methylbutanoate (5.25 mmol) in absolute EtOH (40 mL). The reaction mixture was stirred for 1 h at reflux and overnight at room temperature. The suspension was filtered, and the organic solvent was evaporated in vacuo to give a yellow solid which was dissolved in ethyl acetate. The solution was washed with brine, dried over Na_2SO_4, and the organic solvent was evaporated to dryness, affording the desired compound in quantitative yield as a yellow oil. The resulting amine was used in the next step without any further purification.

Preparation of (+)-*R*- or (−)-*S*-Methyl 2-[4-(2-Heptanoylamino-ethyl)phenoxy]-2-methylbutanoate (*R*-4, *S*-4). Heptanoic acid (7.51 mmol), HOBT·xH_2O (2.48 mmol), and DIC (10.02 mmol) were added to a solution of *R*- or *S*-methyl 2-[4-(2-amino-ethyl)phenoxy]-2-methylbutanoate (5.01 mmol) in CH_2Cl_2 (40 mL). The reaction mixture was stirred for 15 h at room temperature. The organic phase was washed with $NaHCO_3$ saturated solution, 1 N HCl, and brine and then dried over Na_2SO_4 and filtered. The solvent was evaporated to dryness, affording a yellow oily residue which was chromatographed on a silica gel column (petroleum ether/ethyl acetate from 6:4 to 4:6 as eluents) to give the desired compound as a yellow oil.

Preparation of *R*- or *S*-Methyl 2-{4-[2-(*N*-heptyl-*N*-(benzoxazol-2-yl)amino-ethyl)]phenoxy}-2-methylbutanoate (Steps h and i, Scheme 1). One M BH_3 in THF solution (14 mmol) was added, under N_2 atmosphere, to a stirred solution of ***R*-** or ***S*-4** (1.68 mmol) in anhydrous THF (15 mL). The reaction mixture was stirred overnight at room temperature and then was carefully added with MeOH (15 mL) and stirred for 0.5 h at reflux. The organic solvent was evaporated to give an oily residue, which was dissolved in THF (15 mL) and cooled to 0 °C. $N(Et)_3$ (0.2 mL) and a solution of 2-chlorobenzoxazole (2.20 mmol) in anhydrous THF (5 mL) were added to the so-obtained solution. The resulting reaction mixture was stirred for 0.5 h at 0 °C, 0.5 h at room temperature, 2 h at reflux, and 15 h at room temperature. The organic solvent was evaporated to dryness, affording a solid residue which was chromatographed on a silica gel column (petroleum ether/ethyl acetate 9:1 as eluent) to give the title compound as a yellow oil.

Preparation of the Final Acids *R*-1 and *S*-1. A solution of the corresponding methyl ester (0.86 mmol), obtained from the previous steps, in EtOH (10 mL) and 1 N NaOH (5 mL) was stirred for 4 h at room temperature. The organic solvent was removed under reduced pressure and the aqueous phase was acidified with 3 N HCl and extracted with CH_2Cl_2. The organic layer was dried over Na_2SO_4, filtered, and evaporated to dryness, affording an oily residue which was chromatographed on a silica gel column (petroleum ether/ethyl acetate 8:2 and then petroleum ether/ethyl acetate/MeOH 7.5:2:0.5 as eluents) to give the title compound as a white solid, which was recrystallized from Et_2O/*n*-hexane.

Preparation of *R*-2-(4-Nitro-phenoxy)-2-methylbutanoic Acid (5). *R*-2-Hydroxy-2-methylbutanoic acid was obtained by fractional crystallization of its diastereomeric salts with brucine, following a procedure reported in the literature.[25,26] Afterward, a solution of *R*-2-hydroxy-2-methylbutanoic acid (1.79 g, 15.21 mmol) in anhydrous DMF (10 mL) was added, under N_2 atmosphere, to an ice-bath cooled suspension of 95% NaH powder (1.10 g, 45.6 mmol) in the same anhydrous solvent (20 mL). After 0.5 h at 0 °C, a solution of 4-nitro-fluoro-benzene (2.14 g, 15.2 mmol) in anhydrous DMF (15 mL) was added to the reaction mixture, which was stirred overnight at room temperature. Ethyl acetate (20 mL) was added to quench the reaction mixture, and then the organic solvent was distilled off and 6 N HCl was added to the residue and extracted with ethyl acetate. The resulting solution was washed with NH_4Cl saturated solution and brine, and then the organic phase was dried over Na_2SO_4 and the solvent was removed under reduced pressure to give the title compound as a red oil in 85% yield. GC/MS of the methyl ester, *m*/*z* (%): 253 (8) [M^+], 115 (100). This acid was used in the next step without any further purification.

Preparation of (+)-*R*-2-(4-Bromo-phenoxy)-2-methylbutanoic Acid (*R*-2, Steps b and c, Scheme 2). A solution of acid **5** (3.09 g, 12.21 mmol) in MeOH (160 mL) was added to a stirred suspension of 5% Pd (0.1 g) in MeOH (5 mL). The resulting mixture was stirred at room temperature under H_2 atmosphere (4 atm) for 4 h. The suspension was filtered through a celite pad to remove the catalyst and the solvent was evaporated to dryness, affording a dark solid residue, which was readily used in the following step. This intermediate was dissolved in H_2O (15 mL) and 48% HBr (15 mL), and the resulting mixture was cooled to 0 °C and added with a solution of $NaNO_2$ (0.6 g, 8.70 mmol) in H_2O (15 mL).

The reaction mixture was stirred for 0.5 h at 0 °C and then added with a solution of CuBr (3.42 g, 23.84 mmol) in H_2O (30 mL) and 48% HBr (25 mL). The resulting mixture was heated for 1.5 h at 80 °C and stirred overnight at room temperature; afterward, a 50% KOH solution (15 mL) was carefully added up to pH 10. The suspension was filtered through a celite pad, and the aqueous filtrate was washed with CH_2Cl_2, acidified with 6 N HCl and extracted with $CHCl_3$. The collected organic layers were dried over Na_2SO_4, and the solvent was removed under reduced pressure to give the title compound as a colorless oil in 70% yield. ($[\alpha]_D$ = +17, *c* 1, MeOH).

Coregulator Interaction Assays by Fluorescence Resonance Energy Transfer (FRET) Assay. The ligand binding domain (LBD) of human PPARγ was expressed as N-terminal His-tagged protein using a pET28a vector and purified as previously

described.[23] In brief, freshly transformed *Escherichia coli* BL21 DE3 were grown in LB medium with 30 μg of kanamycin $\times$ mL^{-1} at 37 °C to an OD of 0.6. The culture was then induced with 0.1 mM isopropyl-β-D-thiogalactopyranoside and further incubated at 18 °C for 20 h. Cells were harvested and resuspended in a 20 mL $\times$ L^{-1} culture of buffer A (20 mM Tris, 150 mM NaCl, 10% glycerol, 1 mM Tris 2-carboxyethylphosphine HCl, pH 8) in the presence of protease inhibitors (Complete Mini EDTA-free; Roche Applied Science). Cells were sonicated, and the soluble fraction was isolated by centrifugation (35000*g* for 45 min). The supernatant was loaded onto a Ni^{2+}-nitrilotriacetic acid column (GE Healthcare) and eluted with a gradient of imidazole 0−300 mM in buffer A with a PU980 HPLC system (Jasco, Lecco, Italy). The fractions containing the protein were collected, quantitated with a Bradford assay, and analyzed on 12% SDS-PAGE. The protein was then dialyzed over buffer C (20 mM Tris, 20 mM NaCl, 10% glycerol, 1 mM Tris 2-carboxyethylphosphine HCl, pH 8) to remove imidazole. The identity of the His-tagged protein was determined on the basis of the molecular weight and of the sequencing of the tryptic peptides obtained by liquid chromatography−electrospray ionization mass spectrometry and tandem mass spectrometry (data not shown) (LTQ; ThermoElectron Co., San Jose, CA), respectively. The protein was then loaded onto a Q-Sepharose HP column (GE Healthcare) and eluted with a gradient of NaCl 0−500 mM in buffer B (20 mM Tris, 10% glycerol, 1 mM Tris 2-carboxyethylphosphine HCl, pH 8). The protein was then dialyzed over buffer B and kept frozen in aliquots at a concentration of 1 mg·mL^{-1}.

Fluorescence resonance energy transfer assays to evaluate peptide recruitment were performed in 384-well plates in a final volume of 10 μL. A mix of 8 ng of human PPARγ−LBD, 0.8 ng of europium-labeled anti-His antibody (Perkin-Elmer, Monza, Italia), and 86 ng of allophycocyanin-labeled streptavidin (Perkin-Elmer), in a FRET buffer containing 50 mM Tris pH 7.5, 50 mM KCl, 1 mM DTT, and 0.1% free fatty acids BSA was prepared. The tested ligands were added to the mix at the concentration ensuring the saturation of the receptor. The biotinylated peptides (PRIMM, Milano, Italia) were added in 12-point dose response curves starting at 9 μM as the highest concentration. The reactions were equilibrated for 1 h at room temperature and then measured in an Envision multiplate reader (Perkin-Elmer) using 340 nm as excitation and 615 and 665 nm as emission wavelengths. The ratio between 665 (APC signal) and 615 (europium signal) was used to evaluate the peptide recruitment on the receptor.

The peptide sequences used are Biotin-CPSSHSSLTERHKILHRLLQEGSPS-COOH (NR box 2) for SRC-1 spanning from amino acid 676 to 700 (reference number NP_671766), Biotin-DGTPPPQEAEEPSLLKKLLLAPANT-COOH (NR box 1) for PGC-1α spanning from amino acid 130 to 154 (reference number NP_037393), Biotin-LERNNIKQAANNSLLLHLLKSQTIP-COOH (NR box 4) spanning from amino acid 366 to 390, and Biotin-PVSPQDFSFSKNGLLSRLLRQNQDSYL-COOH (NR box 7) spanning from amino acid 805 to 831 for RIP140 (reference number NP_003480), Biotin-SGNLVPDAASKHKQLSELLRGGSGS-COOH (NR box 1) spanning from amino acid 56 to 80 and Biotin-SVQPPRSISPSALQDLLRTLKSP-COOH (NR box 4) spanning from amino acid 2055 to 2078 for CBP (reference number NP_004371), Biotin-GSTHGTSLKEKHKILHRLLQDSSSPVDCOOH (NR box 2) for TIF2 spanning from amino acid 676 to 702 (reference number NP_006531), Biotin-SFADPASNLGLEDIIRKALMGSFDD-COOH (NR box 1) for N-CoR1 spanning from amino acid 2253 to 2277 (reference number NP_006302), and Biotin-APGVKGHQRVVTLAQHISEVITQ-COOH (NR box 1) for SMRT spanning from amino acid 2123 to 2145 (reference number NP_006303).

Chromatin Immunoprecipitation Assays. Murine macrophage cells RAW264.7 were seeded in 10 cm plates and were treated with the indicated compounds. The treatments were performed in triplicate. Sixteen hours after the ligand addition, cells were fixed by adding 1 mL of fixation buffer (500 mM HEPES/KOH, pH 7.9, 100 mM NaCl, 1 mM EDTA, 0.5 mM EGTA, 11% formaldehyde) for 10 min and then washed twice with PBS. Cells were scraped and pelleted for 5 min at 1000*g* at 4 °C. Cells were subsequently lysed in 300 μL of lysis buffer (50 mM Tris, pH8, 5 mM EDTA, pH8, 1% SDS, Complete Mini, Roche). The lysates were homogenized by sonicating on ice with five pulses of 10 s at a power setting of 10 (SONOPULS Bandelin, Berlin Germany) sonicator. Samples were then diluted by adding 1.7 mL of dilution buffer (20 mM TrisHCl, pH8, 100 mM NaCl, 2 mM EDTA, pH8, 0.5% Triton X-100, Complete Mini, Roche). At this point, 200 μL per samples were kept as input. The lysates were precleared by adding 50 μL of Protein-G Sepharose (Amersham) with salmon sperm DNA and incubated 2 h at 4 °C on a rotating shaker. Supernatants were collected and each sample was split in three parts: in the first, we added 5 μg of antibody recognizing N-CoR1 (sc-8994 Santa Cruz Biotechnology, CA), the second one was incubated with 5 μg of general IgG, and the last one with no antibody. All the samples were rotated overnight at 4 °C. Further, the complexes were recovered by adding 50 μL of Protein-G Sepharose with salmon sperm DNA by rotating them for 1 h at 4 °C. The immunoprecipitated DNA was then washed and eluted twice with 100 μL of elution buffer incubating 20 and 10 min, respectively, and shaking the beads every 5 min. The cross-linking was reversed incubating samples at 65 °C for at least 6 h. Samples were incubated with 1 μL of proteinase K for 1 h at 55 °C. The DNAs were cleaned by Qiaquick columns (Qiagen) and eluted in 50 μL of H_2O. DNA samples were analyzed by real time qPCR using 1 μL per reaction following the SYBR green protocol. The primers used are shown in Table 1 of Supporting Information and were those already described by Lefterova et al. and Araki et al.[39,40]

Transfection Assays and Mutation Analysis. The expression plasmids for PPARγ−LBD fused in frame with the Gal4 DNA binding domain (pGal4−PPARγ−LBD) and the reporter vector containing five copies of the Gal4 upstream activating sequences (pGal4UAS-luciferase) driving the transcription of the luciferase reporter gene were kindly donated by Dr. Krister Bamberg (AstraZeneca, Mölndal, Sweden). The expression vectors for PGC-1α, RIP140, CBP, and N-CoR1 were kindly provided by Anastasia Kralli (The Scripps Research Institute, La Jolla, CA), Iannis Talianidis (Biomedical Sciences Research Center "Alexander Fleming", Vari, Greece), and Serena Ghisletti (Istituto FIRC di Oncologia Molecolare, Milano, Italia), respectively. The mutants Q286A, Q286D, Q286E, Q286K, and Q286M were prepared using the QuikChange site-directed mutagenesis kit (Stratagene, La Jolla, CA) and confirmed by automated sequencing. pCMV-GFP, containing the green fluorescent protein gene driven by the cytomegalovirus early promoter/enhancer, was used as an internal standard to normalize for transfection efficiency across wells. For transactivation assays, HEK293T cells (American Type Culture Collection, Manassas, VA) were transfected in suspension with 10 ng of pUAS5XGal4-Luc, 10 ng of receptor expressing vector, 10 ng of coregulator expression vector, 10 ng of pCMV-GFP, and 160 ng of pCDNA3 for a total of 200 ng of DNA per well, using Fugene 6 (Roche, Milano, Italia) as a transfection reagent.[41] Transfected cells (4×10^4) were then seeded in 96-well plates. Four hours after transfection, cells were treated with 5 μM of the indicated compounds in Dulbecco's Modified Eagle Medium, (Invitrogen, Milano, Italy) containing 100 U penicillin G $\times$ mL^{-1}, 100 μg of streptomycin sulfate $\times$ mL^{-1}, and 10% charcoal stripped fetal bovine serum (Euroclone, Milano, Italia). Green fluorescence protein intensity was assessed by bottom reading of the plated living cells using a plate reader (Envision, Perkin-Elmer). Then luciferase activity in cell extracts was determined after 20 h with a luciferase detection kit (Perkin-Elmer, Monza, Italia) using a plate reader luminometer (Envision, Perkin-Elmer).[37] Transfection experiments were performed in triplicates.

Computational Chemistry. Molecular modeling and graphics manipulations were performed using the molecular operating environment (MOE)[38] and UCSF-CHIMERA software packages,[42] running on a 2 CPU (PIV 2.0−3.0 GHZ) Linux workstation. Energy minimizations were realized by employing the AMBER 9 program,[43] selecting the Cornell et al. force field.[44] Molecular modeling calculations were based on the X-ray structure coordinates of the complexes of the ligand-free PPARγ (PDB code 1PRG)[36] and the rosiglitazone- (PDB code 2PRG),[36] ***S*-1**- (PDB code 2I4P)[23] and ***R*-1**-bound (PDB code 2I4J)[23] structure, deposited in the Protein Data Bank (PDB). The mutations at position 286 were accomplished by the MOE Rotamer Explorer function. The resulting mutants Q286E, Q286A, Q286K, Q286M, and Q286D models were then solvated with water molecules in a truncated octahedron periodic box. The distance between the box walls and the protein was set to 10.0 Å, which resulted in about 13000 water molecules for each system. The TIP3P water model was used.[45] The systems were neutralized by adding the corresponding number of counterions. Energy minimization was conducted in three steps. First, only water molecules and ions were allowed to move. Next, the movement was extended to the residues within 5.0 Å around the mutated residue. Finally, all atoms were allowed to move freely. In each step, energy minimization was carried out by a combination of the steepest descent method for 5000 steps and the conjugated gradient method for another 5000 steps.

PPARγ and the related complexes with ***R*-1** and ***S*-1** have been investigated in aqueous solution by means of MD simulations using the GROMACS package.[46] Each system was initially placed in a rectangular box of 866 nm^3 with 27480 water molecules described by the single point charge (SPC)[47] and six counterions (Na^+). The dimension of the box was selected in order to avoid any interaction of the solute with its replica, which could arise from the application of periodic boundary conditions. Rototranslational constraints were applied to the solute for obtaining correct statistical mechanics and thermodynamics.[48] For all the investigated systems, we used the same initial coordinates, taken from the PPARγ−***R*-1** crystal complex (PDB code 2I4J).[23] The following protocol was adopted for all the simulations: the systems were initially minimized by using a standard steepest descent algorithm; then, after solvation and the initial equilibration of the solvent, each system was relaxed for 100 ps in an isothermal/isobaric ensemble to obtain the correct density of the water. Each simulation was finally carried out in an isothermal/isochoric ensemble at 300 K for about 15.3 ns using an integration step of 2.0 fs. For each simulation, the first part of trajectory (0.5−2.0 ns) was discarded basing on the Cα root-mean-square deviations and only the last 14.0 ns of each trajectory were analyzed. The temperature was kept constant by the isokinetic temperature coupling.[49] All bond lengths were constrained using LINCS.[50] The long-range electrostatics was computed by the particle mesh Ewald method,[51] with 34 wave vectors in each dimension and a fourth-order cubic interpolation. Gromos force field[52] parameters were adopted for the receptor, while the Lennard-Jones parameters of similar atoms were considered for the ligands.

Acknowledgment. We thank Dr. Krister Bamberg (AstraZeneca, Mölndal, Sweden) for kindly providing the Gal4−PPARγ vector and pET28a−PPARγ−LBD expression vector and Drs. Anastasia Kralli (The Scripps Research Institute, La Jolla, CA), Iannis Talianidis (Biomedical Sciences Research Center "Alexander Fleming", Vari, Greece), and Serena Ghisletti (Istituto FIRC di Oncologia Molecolare, Milano, Italia) for the kind gift of the expression vectors for PGC-1α, RIP140, CBP, and N-CoR1. We also thank Dr. Cristina Godio for expression and purification and Dr. Donatella Caruso for mass spectrometry analysis of His-tagged PPARγ LBD. We are also grateful to Elda Desiderio Pinto (Università degli Studi di Milano) for administrative and financial management. This work was supported by The Giovanni Armenise−Harvard Foundation Career Development Grant (NM), by the CARIPLO Foundation (FG), by grants from the Università degli Studi di Milano (MC) and Università degli Studi di Bari "Aldo Moro" and by a donation from the Francesco Del Gaudio family.

Supporting Information Available: Yields, physicochemical properties, and spectroscopic data for intermediates and final compounds; molecular dynamics, molecular modeling, and biological data. This material is available free of charge via the Internet at http://pubs.acs.org.

References

(1) Rosen, E. D.; Spiegelman, B. M. PPARgamma: a nuclear regulator of metabolism, differentiation, and cell growth. *J. Biol. Chem.* **2001**, *276*, 37731–37734.
(2) Nuclear Receptors Nomenclature Committee. A unified nomenclature system for the nuclear receptor superfamily. *Cell* **1999**, *97*, 161−163.
(3) Evans, R. M.; Barish, G. D.; Wang, Y. X. PPARs and the complex journey to obesity. *Nat. Med.* **2004**, *10*, 355–361.
(4) Semple, R. K.; Chatterjee, V. K.; O'Rahilly, S. PPAR gamma and human metabolic disease. *J. Clin. Invest.* **2006**, *116*, 581–589.
(5) Forman, B. M.; Tontonoz, P.; Chen, J.; Brun, R. P.; Spiegelman, B. M.; Evans, R. M. 15-Deoxy-delta 12,14-prostaglandin J2 is a ligand for the adipocyte determination factor PPAR gamma. *Cell* **1995**, *83*, 803–812.
(6) Lehmann, J. M.; Moore, L. B.; Smith-Oliver, T. A.; Wilkison, W. O.; Willson, T. M.; Kliewer, S. A. An antidiabetic thiazolidinedione is a high affinity ligand for peroxisome proliferator-activated receptor gamma (PPAR gamma). *J. Biol. Chem.* **1995**, *270*, 12953–12956.
(7) Olefsky, J. M.; Saltiel, A. R. PPAR gamma and the treatment of insulin resistance. *Trends Endocrinol. Metab.* **2000**, *11*, 362–368.
(8) Staels, B. PPAR agonists and the metabolic syndrome. *Therapie* **2007**, *62*, 319–326.
(9) Willson, T. M.; Cobb, J. E.; Cowan, D. J.; Wiethe, R. W.; Correa, I. D.; Prakash, S. R.; Beck, K. D.; Moore, L. B.; Kliewer, S. A.; Lehmann, J. M. The structure−activity relationship between peroxisome proliferator-activated receptor gamma agonism and the antihyperglycemic activity of thiazolidinediones. *J. Med. Chem.* **1996**, *39*, 665–668.
(10) Nesto, R. W.; Bell, D.; Bonow, R. O.; Fonseca, V.; Grundy, S. M.; Horton, E. S.; Le Winter, M.; Porte, D.; Semenkovich, C. F.; Smith, S.; Young, L. H.; Kahn, R. Thiazolidinedione use, fluid retention, and congestive heart failure: a consensus statement from the American Heart Association and American Diabetes Association. *Diabetes Care* **2004**, *27*, 256–263.
(11) Bodmer, M.; Meier, C.; Kraenzlin, M. E.; Meier, C. R. Risk of fractures with glitazones: a critical review of the evidence to date. *Drug. Saf.* **2009**, *32*, 539–547.
(12) Berger, J. P.; Petro, A. E.; Macnaul, K. L.; Kelly, L. J.; Zhang, B. B.; Richards, K.; Elbrecht, A.; Johnson, B. A.; Zhou, G.; Doebber, T. W.; Biswas, C.; Parikh, M.; Sharma, N.; Tanen, M. R.; Thompson, G. M.; Ventre, J.; Adams, A. D.; Mosley, R.; Surwit, R. S.; Moller, D. E. Distinct properties and advantages of a novel peroxisome proliferator-activated protein [gamma] selective modulator. *Mol. Endocrinol.* **2003**, *17*, 662–676.
(13) Acton, J. J., III; Black, R. M.; Jones, A. B.; Moller, D. E.; Colwell, L.; Doebber, T. W.; Macnaul, K. L.; Berger, J.; Wood, H. B. Benzoyl 2-methyl indoles as selective PPARgamma modulators. *Bioorg. Med. Chem. Lett.* **2005**, *15*, 357–362.
(14) Dropinski, J. F.; Akiyama, T.; Einstein, M.; Habulihaz, B.; Doebber, T.; Berger, J. P.; Meinke, P. T.; Shi, G. Q. Synthesis and biological activities of novel aryl indole-2-carboxylic acid analogs as PPARgamma partial agonists. *Bioorg. Med. Chem. Lett.* **2005**, *15*, 5035–5038.
(15) Minoura, H.; Takeshita, S.; Ita, M.; Hirosumi, J.; Mabuchi, M.; Kawamura, I.; Nakajima, S.; Nakayama, O.; Kayakiri, H.; Oku, T.; Ohkubo-Suzuki, A.; Fukagawa, M.; Kojo, H.; Hanioka, K.; Yamasaki, N.; Imoto, T.; Kobayashi, Y.; Mutoh, S. Pharmacological characteristics of a novel nonthiazolidinedione insulin sensitizer, FK614. *Eur. J. Pharmacol.* **2004**, *494*, 273–281.
(16) Oberfield, J. L.; Collins, J. L.; Holmes, C. P.; Goreham, D. M.; Cooper, J. P.; Cobb, J. E.; Lenhard, J. M.; Hull-Ryde, E. A.; Mohr, C. P.; Blanchard, S. G.; Parks, D. J.; Moore, L. B.; Lehmann, J. M.; Plunket, K.; Miller, A. B.; Milburn, M. V.; Kliewer, S. A.; Willson, T. M. A peroxisome proliferator-activated receptor gamma ligand

inhibits adipocyte differentiation. *Proc. Natl. Acad. Sci. U.S.A.* **1999**, *96*, 6102–6106.
(17) Burgermeister, E.; Schnoebelen, A.; Flament, A.; Benz, J.; Stihle, M.; Gsell, B.; Rufer, A.; Ruf, A.; Kuhn, B.; Marki, H. P.; Mizrahi, J.; Sebokova, E.; Niesor, E.; Meyer, M. A novel partial agonist of peroxisome proliferator-activated receptor-gamma (PPARgamma) recruits PPARgamma-coactivator-1alpha, prevents triglyceride accumulation, and potentiates insulin signaling in vitro. *Mol. Endocrinol.* **2006**, *20*, 809–830.
(18) Bruning, J. B.; Chalmers, M. J.; Prasad, S.; Busby, S. A.; Kamenecka, T. M.; He, Y.; Nettles, K. W.; Griffin, P. R. Partial agonists activate PPARgamma using a helix 12 independent mechanism. *Structure* **2007**, *15*, 1258–1271.
(19) Nettles, K. W. Insights into PPARgamma from structures with endogenous and covalently bound ligands. *Nat. Struct. Mol. Biol.* **2008**, *15*, 893–895.
(20) Xu, H. E.; Li, Y. Ligand-dependent and -independent regulation of PPAR gamma and orphan nuclear receptors. *Sci. Signal.* **2008**, *1*, 52.
(21) Li, Y.; Zhang, J.; Schopfer, F. J.; Martynowski, D.; Garcia-Barrio, M. T.; Kovach, A.; Suino-Powell, K.; Baker, P. R.; Freeman, B. A.; Chen, Y. E.; Xu, H. E. Molecular recognition of nitrated fatty acids by PPAR gamma. *Nat. Struct. Mol. Biol.* **2008**, *15*, 865–867.
(22) Chandra, V.; Huang, P.; Hamuro, Y.; Raghuram, S.; Wang, Y.; Burris, T. P.; Rastinejad, F. Structure of the intact PPAR-gamma-RXR-alpha nuclear receptor complex on DNA. *Nature* **2008**, *456*, 350–356.
(23) Pochetti, G.; Godio, C.; Mitro, N.; Caruso, D.; Galmozzi, A.; Scurati, S.; Loiodice, F.; Fracchiolla, G.; Tortorella, P.; Laghezza, A.; Lavecchia, A.; Novellino, E.; Mazza, F.; Crestani, M. Insights into the mechanism of partial agonism: crystal structures of the peroxisome proliferator-activated receptor gamma ligand-binding domain in the complex with two enantiomeric ligands. *J. Biol. Chem.* **2007**, *282*, 17314–17324.
(24) Montanari, R.; Saccoccia, F.; Scotti, E.; Crestani, M.; Godio, C.; Gilardi, F.; Loiodice, F.; Fracchiolla, G.; Laghezza, A.; Tortorella, P.; Lavecchia, A.; Novellino, E.; Mazza, F.; Aschi, M.; Pochetti, G. Crystal structure of the peroxisome proliferator-activated receptor gamma (PPARgamma) ligand binding domain complexed with a novel partial agonist: a new region of the hydrophobic pocket could be exploited for drug design. *J. Med. Chem.* **2008**, *51*, 7768–7776.
(25) Mattocks, A. R. Novel reactions of some α-acyloxy acid chlorides. *J. Chem. Soc.* **1964**, 1918–1930.
(26) Christensen, B. W.; Kjaer, A. The Absolute Configuration of 2-Hydroxy-2-methylbutyric Acid. *Acta Chem. Scand.* **1962**, *16*, 2466–2467.
(27) Xu, H. E.; Stanley, T. B.; Montana, V. G.; Lambert, M. H.; Shearer, B. G.; Cobb, J. E.; McKee, D. D.; Galardi, C. M.; Plunket, K. D.; Nolte, R. T.; Parks, D. J.; Moore, J. T.; Kliewer, S. A.; Willson, T. M.; Stimmel, J. B. Structural basis for antagonist-mediated recruitment of nuclear co-repressors by PPARalpha. *Nature* **2002**, *415*, 813–817.
(28) Amadei, A.; Linssen, A. B.; Berendsen, H. J. Essential dynamics of protein. *Proteins* **1993**, *17*, 412–425.
(29) Davies, S. S.; Pontsler, A. V.; Marathe, G. K.; Harrison, K. A.; Murphy, R. C.; Hinshaw, J. C.; Prestwich, G. D.; Hilaire, A. S.; Prescott, S. M.; Zimmerman, G. A.; McIntyre, T. M. Oxidized alkyl phospholipids are specific, high affinity peroxisome proliferator-activated receptor gamma ligands and agonists. *J. Biol. Chem.* **2001**, *276*, 16015–16023.
(30) Nagy, L.; Schwabe, J. W. Mechanism of the nuclear receptor molecular switch. *Trends Biochem. Sci.* **2004**, *29*, 317–324.
(31) Albers, M.; Blume, B.; Schlueter, T.; Wright, M. B.; Kober, I.; Kremoser, C.; Deuschle, U.; Koegl, M. A novel principle for partial agonism of liver X receptor ligands. Competitive recruitment of activators and repressors. *J. Biol. Chem.* **2006**, *281*, 4920–4930.
(32) Phelan, C. A.; Weaver, J. M.; Steger, D. J.; Joshi, S.; Maslany, J. T.; Collins, J. L.; Zuercher, W. J.; Willson, T. M.; Walker, M.; Jaye, M.; Lazar, M. A. Selective partial agonism of liver X receptor alpha is related to differential corepressor recruitment. *Mol. Endocrinol.* **2008**, *22*, 2241–2249.
(33) Treuter, E.; Albrektsen, T.; Johansson, L.; Leers, J.; Gustafsson, J. A. A regulatory role for RIP140 in nuclear receptor activation. *Mol. Endocrinol.* **1998**, *12*, 864–881.
(34) Klein, F. A.; Atkinson, R. A.; Potier, N.; Moras, D.; Cavarelli, J. Biochemical and NMR mapping of the interface between CREB-binding protein and ligand binding domains of nuclear receptor: beyond the LXXLL motif. *J. Biol. Chem.* **2005**, *280*, 5682–5692.
(35) Molnar, F.; Matilainen, C.; Carlberg, J. Structural determinants of the agonist-independent association of human peroxisome proliferator-activated receptors with coactivators. *J. Biol. Chem.* **2005**, *280*, 26543–26556.
(36) Nolte, R. T.; Wisely, G. B.; Westin, S.; Cobb, J. E.; Lambert, M. H.; Kurokawa, R.; Rosenfeld, M. G.; Willson, T. M.; Glass, C. K.; Milburn, M. V. Ligand binding and co-activator assembly of the peroxisome proliferator-activated receptor-gamma. *Nature* **1998**, *395*, 137–143.
(37) Bower, M. J.; Cohen, F. E.; Dunbrack, R. L., Jr. Prediction of protein side-chain rotamers from a backbone-dependent rotamer library: a new homology modeling tool. *J. Mol. Biol.* **1997**, *267*, 1268–1282.
(38) *Molecular Operating Environment* (*MOE*), version 2005.06; Chemical Computing Group, Inc.: Montreal, 2005.
(39) Lefterova, M. I.; Zhang, Y.; Steger, D. J.; Schupp, M.; Schug, J.; Cristancho, A.; Feng, D.; Zhuo, D.; Stoeckert, C. J., Jr.; Liu, X. S.; Lazar, M. A. PPARgamma and C/EBP factors orchestrate adipocyte biology via adjacent binding on a genome-wide scale. *Genes Dev.* **2008**, *22*, 2941–2952.
(40) Araki, O.; Ying, H.; Furuya, F.; Zhu, X.; Cheng, S. Y. Thyroid hormone receptor beta mutants: dominant negative regulators of peroxisome proliferator-activated receptor gamma action. *Proc. Natl. Acad. Sci. U.S.A.* **2005**, *102*, 16251–16256.
(41) De Fabiani, E.; Nitro, M.; Gilardi, F.; Caruso, D.; Crestani, M. Coordinated control of cholesterol catabolism to bile acids and of gluconeogenesis via a novel mechanism of transcription regulation linked to the fasted-to-fed cycle. *J. Biol. Chem.* **2003**, *278*, 39124–39132.
(42) Huang, C. C.; Couch, G. S.; Pettersen, E. F.; Ferrin, T. E. Chimera: an extensible molecular modeling application constructed using standard components. *Pac. Symp. Biocomput.* **1996**, *1*, 724 http://www.cgl.ucsf.edu/chimera.
(43) Case, D. A.; Darden, T. A.; Cheatham, T. E., III; Simmerling, C. L.; Wang, J.; Duke, R. E.; Luo, R.; Merz, K. M.; Pearlman, D. A.; Crowley, M.; Walker, R. C.; Zhang, W.; Wang, B.; Hayik, S.; Roitberg, A.; Seabra, G.; Wong, K. F.; Paesani, F.; Wu, X.; Brozell, S.; Tsui, V.; Gohlke, H.; Yang, L.; Tan, C.; Mongan, J.; Hornak, V.; Cui, G.; Beroza, P.; Mathews, D. H.; Schafmeister, C.; Ross, W. S.; Kollman, P. A. *AMBER 9*; University of California: San Francisco, 2006.
(44) Cornell, W. D.; Cieplak, P.; Bayly, C. I.; Gould, I. R.; Merz, K. M., Jr.; Ferguson, D. M.; Spellmeyer, D. C.; Fox, T.; Caldwell, J. W.; Kollman, P. A. A second generation force field for the simulation of proteins, nucleic acids, and organic molecules. *J. Am. Chem. Soc.* **1995**, *117*, 5179–5197.
(45) Jorgensen, W. L.; Chandrasekhar, J.; Madura, J.; Klein, M. L. Comparison of simple potential functions for simulating liquid water. *J. Chem. Phys.* **1983**, *79*, 926–935.
(46) Van der Spoel, D.; van Buren, A. R.; Apol, E.; Meulenhoff, P. J.; Tieleman, D. P.; Sijbers, A. L. T. M.; van Drunen, R.; Berendsen, H. J. C. *Gromacs User Manual*, version 1.3, **1996**.
(47) Berendsen, H. J. C.; Postma, J. P. M.; van Gunsteren, W. F. Hermans interaction models for water in relation to protein hydration. In *Intermolecular Forces*; Pullman, B., Ed.; Reidel Publishing Company: Dordrecht, The Netherlands, 1981; pp 331−342.
(48) Amadei, A.; Chillemi, G.; Ceruso, M.; Grottesi, A.; Di Nola, A. Molecular dynamics simulations with constrained roto-translational motions: theoretical basis and statistical mechanical consistency. *J. Chem. Phys.* **2000**, *112*, 9–23.
(49) Berendsen, H. J. C.; Postma, J. P. M.; van Gunsteren, W. F.; Di Nola, A. Molecular dynamics with coupling to an external bath. *J. Chem. Phys.* **1984**, *81*, 3684–3690.
(50) Hess, B.; Bekker, H.; Berendsen, H. J. C.; Frajie, J. G. E. M. LINCS: a linear constraint solver for molecular simulations. *J. Comput. Chem.* **1997**, *18*, 1463–1472.
(51) Darden, T. A.; York, D. M.; Pedersen, L. G. Particle mesh Ewald: method for Ewald sums in large systems. *J. Chem. Phys.* **1993**, *98*, 10089–10092.
(52) van Gunsteren, W. F.; Billeter, S. R.; Eising, A. A.; Hunemberger, P. H.; Kruger, P.; Mark, A. E.; Scott, V. R. P.; Tironi, I. G. *Biomolecular Simulations: The GROMOS96 Manual and User Guide*; vdf Hochschlverlag AG an der ETH Zurich: Zurich, 1996.